Spatiotemporal variability of droughts in the Congo River Basin: The role of atmospheric moisture transport

R. Sorí[1, 2], M. Stojanovic[2], R. Nieto[1], M. L. R. Liberato[2,3] and L. Gimeno[1]

[1]Environmental Physics Laboratory (EPhysLab), CIM-UVigo, Universidade de Vigo, 32004 Ourense, Spain

[2]Instituto Dom Luiz, Faculdade de Ciências, Universidade de Lisboa, 1749-016 Campo Grande, Portugal

[3]Escola de Ciências e Tecnologia, Universidade de Trás-os-Montes e Alto Douro, 5001-801 Vila Real, Portugal

Corresponding author: R.Sorí
Email: rogert.sori@uvigo.es

Keywords

Drought, Moisture transport, Congo River Basin

Abstract

The spatiotemporal evolution of droughts in the Congo River Basin (CRB) from 1981–2018 was investigated using the Standardised Precipitation Index (SPI) and Standardised Precipitation–Evapotranspiration Index (SPEI) to assess the roles of precipitation and potential evapotranspiration. The results confirmed a notable trend toward drier conditions, particularly in parts of the northern and central basin, as well as in the south of the CRB, which was associated with increases in potential evapotranspiration and declining rainfall. Global outputs of the Lagrangian model FLEXPART were used to model air masses over four important climatological regions considered to be the main sources of precipitation in the CRB, and their contributions to precipitation over the basin were computed. These analyses confirmed that moisture in the CRB is ~60% self-sourced; African lands were the next greatest contributor, followed by the Indian and Atlantic Oceans. It was found that a reduction in contributions of the sources prevailed during 53 meteorological drought episodes that affected the CRB during the study period and it could be inferred that a reduction in moisture supplied from the Atlantic and Indian Oceans played an important role in the onset of drought episodes. It was also observed that the contribution of moisture from all sources to the CRB decreased during the study period, especially over the northern half of the basin, where the main humid forest of the CRB is located, confirming the importance of water transport and local hydroclimatological dynamics on the hydrological conditions, ecosystems, and local communities of the CRB.

1. Introduction

Droughts are one of the major natural disasters worldwide, especially in Africa, where droughts affect millions of people (Niang et al., 2014; Gautier et al., 2016). Many studies based on instrumental records in Africa have indicated that droughts have become more frequent, intense, and widespread over the last 50 years (Masih et al., 2014). Most of the African continent is semi-arid and prone to extreme variations in yearly rainfall (Nicholson et al., 2018), though droughts can occur in areas of both high and low rainfall (Wilhite and Glantz, 1985). One of the African regions where it rains the most is the Congo River Basin (CRB). It is located in Central Equatorial Africa (CEA), one of the most convective regions on Earth (Washington et al 2013; Chakraborty et al., 2020) and home to one of the densest forests (Dargie et al., 2019). Recent findings have confirmed that CEA has experienced long-term drying since the 1980s (Raghavendra et al., 2020), particularly during April–June (Hua et al., 2016; 2018). Accordingly, a tendency toward a higher percentage of areas experiencing droughts driven by increases in temperature since 1990 has been observed (Spinoni et al., 2019). Observations have also revealed a widespread increase in the length of the boreal summer (June–August) dry season across the CRB since the 1980s, from both hydrological and ecological perspectives; this has primarily been attributed to the earlier onset and delayed termination of the dry season (Jiang et al., 2019). According to previous studies, this earlier onset of the dry season has been caused by long-term droughts due to decreased rainfall in the pre-dry season (April–June). The delayed termination of the dry season is a result of insufficient stocks of soil moisture, which postpones the start of the subsequent wet season and hinders the regrowth of vegetation. Field observations and previous findings for Cameroon, the Central African Republic, and the Democratic Republic of Congo have revealed that the variability in the rainfall regime affects water flow in the CRB. In the three studied watersheds mentioned, temperatures are rising, rainfall is declining, water flow is disturbed, and the livelihoods of rural communities are being negatively affected (Sonwa et al., 2020).

The spatial extent of droughts is usually much greater than that of other natural hazards and their impacts are generally non-structural and difficult to quantify (Serrano and Moreno, 2005). This occurs because there are several definitions of drought, and therefore a great variety of indices and indicators that allow drought conditions to be represented, considering different cumulative time scales. An analysis of the geospatial coverage of selected droughts in Africa from 1900–2013 revealed that they did not always affect all of CEA homogeneously (Masih et al., 2014) and therefore, cropland and forest drought exposure may vary within the CRB (Kamali et al., 2018; Zhou et al., 2014). The mechanisms associated with such variations have been investigated taking into account the hydroclimatic characteristics of the entire region. According to Hua et al. (2016) CEA droughts are primarily related to variations in sea surface temperature over the Indo-Pacific, which are themselves associated with enhanced and westward extended tropical Walker circulation that has reduced low-level moisture transport to CEA, and consequently weakened the ascent of moisture over this region. However, the findings of Sorí et al. (2017) suggested the reduction in the contribution of moisture to the precipitation over the CRB from three important sources: (1) the eastern tropical equatorial South Atlantic Ocean, (2) the eastern Indian Ocean north of Somalia and Ethiopia, along the eastern coast of Africa to approximately 20°S, and (3) the CRB itself during years affected by severe and extreme drought in the CRB. They highlighted that the greatest anomalies in the contribution of moisture were found in air masses from the CRB itself.

The seasonal variability of the spatial gradient of precipitation recycling in CEA is regulated by both the direction and strength of the moisture flux, while annual cycles of the recycling ratio in northern and southern CEA are

regulated by both moisture transport and evapotranspiration (Pokam et al., 2012). The Congo region lacks major mountain ridges to trigger rainfall, thus, the forests sustain atmospheric moisture through evaporation and are of utmost importance for the region's water resources (van der Ent and Savenije, 2011). The atmospheric circulation over the Congo region is largely dependent on the role of vegetation and rainforests, which make it vulnerable to the impacts of anthropogenic changes in vegetation cover (Elthair, 1996). Modelling simulations have confirmed the local and remote effects of the deforestation of the CRB; locally decreased evapotranspiration has reduced precipitation (by up to 50%) over all seasons (Nogherotto et al., 2013). Thus, despite the low rate of deforestation in the CRB (Megevand et al., 2013), the forest loss dominated by increasing smallholder clearing for agriculture (Tyukavina et al., 2018) has played a significant role in changing the local hydrological cycle by exacerbating drought (Wilhite, 1992). In contrast to this view, Bell et al. (2015) argued that precipitation in CEA does not necessarily decrease with decreased evapotranspiration, owing to tropical deforestation, because the reduced evapotranspiration efficiency causes a significant increase in near-surface temperatures, generating an area of low pressures and convergence.

Numerous studies have confirmed the key role of the CRB on the modulation of the local hydroclimatic regime. However, regardless of the increasing number of studies, their remains considerable opportunity for continued research in the CRB, as the Congo is one of the least studied major river basins on Earth (Alsdorf et al., 2016). The results of Gimeno et al. (2020) showed that the greatest amount of precipitation in the CRB originates from a terrestrial origin, and that precipitation from oceanic origins decreased more than the precipitation from terrestrial origins from 1980–2015. Despite these results, the short and long-term roles of moisture contributed for precipitation in the CRB from oceanic and terrestrial regions is still unclear, and compared to precipitation, less information is available regarding evapotranspiration and temperature in the CRB (Alsdorf, et al., 2016). Thus, in this study, we aim to expound upon previous findings by investigating the spatiotemporal variability of droughts in the CRB, considering both precipitation and potential evapotranspiration, and by separately assessing the role of the contributions to precipitation from oceanic and terrestrial moisture sources on the occurrence and severity of short and long-term droughts in the CRB.

1.1 Study area

The CRB (Figure 1), located in CEA, is the second largest river basin worldwide, after the Amazon in South America, and it extends over nine countries: Angola, Cameroon, Central African Republic, Democratic Republic of the Congo, Republic of the Congo, Burundi, Rwanda, Tanzania, and Zambia. Spread across the CRB is the Congo Rainforest, the world's second largest contiguous block of tropical forest, after the Amazon Rainforest, encompassing 400 million hectares, 200 million of which are covered by forest, with 90% being dense tropical forests, representing 70% of all African forestlands (UNESCO, 2010; Megevand et al., 2013). The Congo River (a.k.a., Zaire River) is the fifth longest river in the world, and the second longest in Africa (WWF, 2020). Therefore, the basin is characterised by high levels of biological diversity and endemism of both plant and animal species. Demographic factors are major causes underlying deforestation in the CRB, as they are chiefly associated with the growth of subsistence activities (agriculture and energy) and are strongly correlated with demographic patterns (Megevand et al., 2013).

The geographic location and extent of the CRB in the northern and southern hemispheres allow it to receive rainfall due to the seasonal–south migration of the Intertropical Convergence Zone (Nicholson, 2018). The pattern of precipitation in the basin consists of two rainy seasons, from March–May and from September–November, the latter of which represents the more pronounced rainy season, and a dry season from June–

August (Washington et al., 2013; Dyer et al., 2017; Sorí et al., 2017). This makes the region a complex hydroclimatic region, with several subbasins.

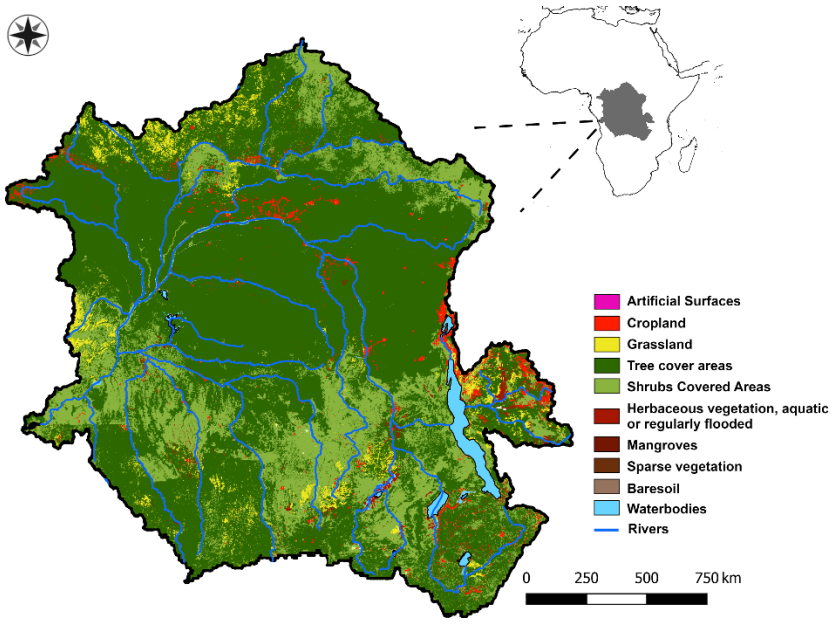

Figure 1. Geographic location of the CRB and the Land cover in 2003 with a grid resolution of 1 Km from the United States Geological Survey. Freely available at: http://www.fao.org/geonetwork/srv

2. Material and methods

2.1 Drought indices

There are many definitions of drought in the scientific literature; for instance, an insidious natural hazard that results from lower levels of precipitation than what is considered normal (WMO, 2012). Therefore, several indices exist for identifying and monitoring drought events, a great number of which are listed and explained in the *Handbook of Drought Indicators and Indices* (WMO-GWP, 2016). Some of the most widely used meteorological drought indices are the Standardised Precipitation Index (SPI) (Mckee et al., 1993), the Palmer Drought Severity Index (Palmer, 1965), and the Standardised Precipitation–Evapotranspiration Index (SPEI) (Vicente-Serrano et al., 2010). In this study, the SPI and SPEI are utilised to investigate the temporal and spatial variability of droughts in the CRB.

The SPI has been widely utilised and recommended by the World Meteorological Organization (WMO) to monitor drought conditions. According to Mckee et al. (1993), to calculate the SPI, a long-term precipitation record of at least 30 years is needed. This series, for the period of interest, is then fitted to a probability distribution that is later transformed into a normal distribution, such that the mean SPIs for the study area and the chosen period are zero (Edwards and McKee, 1997). The SPI was calculated according to a Pearson III distribution to obtain the distribution parameters, following the methods of Vicente-Serrano (2006) and Vicente-Serrano et al. (2010). The Pearson III distribution is a three-parameter model with shape, scale, and location parameters containing asymmetrical distributions that are either positively or negatively skewed; it is closely related to the gamma distribution (Koutrouvelis and Canavos, 1999) and has been widely utilised in statistical analyses across the hydrological sciences. SPI values represent the number of standard deviations by which cumulative precipitation deviates from the climatological

mean. Therefore, positive or negative SPI values indicate wet or dry conditions, respectively. As the SPI is normalised, wetter and drier climates can be represented in the same way; thus, wet periods can also be monitored using the SPI (WMO, 2012).

The SPEI has been utilised over the last decade to investigate drought phenomena in many parts of the world, especially in tropical humid regions. This is because SPEI takes into account both the water supply through the precipitation (*P*), and the atmospheric water demand through the potential evapotranspiration (*PET*) in determining drought conditions. Consequently, an advantage of the SPEI with respect to the SPI is that it provides a more reliable measure of drought severity (Vicente-Serrano et al., 2010; Beguería et al., 2014). The SPEI is based on the same conceptual framework as the SPI. However, the SPEI is derived from the climatic water balance rather than the *P* as the only input, as shown in equation 1:

$$D = P - PET, \tag{1}$$

where *D* values are aggregated at different time scales, according to a similar method as that for the SPI. In the next step *D* series are fit to the most suitable probability distribution. According to Vicente-Serrano et al. (2010) and Beguería et al. (2014), to model *D* values calculated at different time scales, the most suitable distribution is the log–logistic distribution, the formulation whereof is shown in equation 2:

$$F(D) = [1 + (\frac{\alpha}{D-\gamma})^{\beta}]^{-1}, \tag{2}$$

where α, β, and γ are the parameters of scale, shape, and location. The three-parameter log–logistic distribution is a generalisation of the two-parameter log–logistic distribution, for which parameters can be estimated through several methods, and has been applied to frequency analyses of precipitation and streamflow data (Singh, 1998). Following Beguería et al. (2014), model fitting was conducted to plot positions so that they were unbiased using the Probability Weighted Moment. Finally, the SPEI was obtained as standardised values of *F(D)*. Both the SPI and the SPEI were computed for temporal frequencies from 1–24 months. This multiscale characteristic is an advantage because it allows different types of droughts to be recognised. Negative and positive SPEI values indicate drier and wetter conditions, respectively. An advantage of the SPEI over the SPI is that it also avoids issues inherent in the SPI, such as fitting periods with zero precipitation. For the calculation of the SPEI, the R package 'SPEI', available at http://cran.r-project.org/web/packages/SPEI, was utilised, including all of the recommendations proposed by Beguería et al. (2014).

In this study, we used the pre-established drought categories proposed by Agnew (2000) (Table 1)to investigate the temporal and spatial evolution of drought in the CRB. The classification proposed by Mckee et al. (1993) has been used in many studies. However, the classification of Agnew (2000) gives a more realistic estimation based on probability classes rather than the magnitudes of the SPI; because of this difference, we contend that the classification of Agnew (2000) is a more rational approach. Drought episodes were considered to occur (onset) when the SPI or the SPEI fell below zero, reaching a value of at least -0.84, and later returned to positive values (termination). The threshold of -0.84 corresponds to a 20% probability, which means that a drought is only expected twice in 10 years. The SPEI at the temporal scale of one month, in accordance with the WMO (2012), was used to identify meteorological droughts. All such episodes were calculated with respect to their duration and severity. The duration was considered to be the sum of all months within an episode and the severity was considered to be the sum of all absolute

SPEI values during the episode.

Table 1. Drought categories of the SPEI according to Agnew (2000).

SPEI	Probability	Category
> 1.65	0.05	Extremely humid
> 1.28	0.10	Severely humid
> 0.84	0.20	Moderately humid
-0.84 < SPEI < 0.84	0.60	Normal
< -0.84	0.20	Moderately dry
< -1.28	0.10	Severely dry
< -1.65	0.05	Extremely dry

2.2 Flexible Particle Dispersion Model

Global outputs from the Flexible Particle Dispersion Model (FLEXPART) v9.0 (Stohl and James, 2004, 2005) were used to investigate the role of the Atlantic Ocean (AO), Indian Ocean (IO), African continent (without the CRB) (AF), and the CRB itself (Figure 2) as moisture sources for precipitation over the CRB. This model first considers the atmosphere as homogeneously divided into a multiple air parcels (~2.0 million in the simulation used) that can be tracked backward or forward in time. In the forward model, the parcels residing over the aforementioned sources were advected forward in time by three-dimensional wind fields up to 10 days, according to the mean residence time of the water vapour in the atmosphere (Nummaguti et al., 1999) by applying equation 3:

$$\frac{dx}{dt} = v[x(t)], \tag{3}$$

where x is the position of the parcel and v[x(t)] is the wind speed, interpolated in space and time, of the corresponding analytical grid. Along the trajectories, the gain (through evaporation from the environment, e) or loss (through precipitation, p) in specific humidity (q) by each parcel is calculated according to equation 4:

$$(e - p) = m\left(\frac{dq}{dt}\right), \tag{4}$$

where m is the mass of a particle, which was considered to be constant. Phase changes in clouds are included in estimates of ($e - p$), but a problem exists in that fluctuations in q along individual trajectories can arise for nonphysical reasons (e.g. because of q interpolations or trajectory errors); consequently, absolute values of ($e - p$) may be highly biased. According to Stohl and James (2004), part of this noise is compensated for among the many particles in an atmospheric column over area, A. During travel, the target parcels disperse; thus, integrating $(e - p)$ for all the parcels in the atmospheric column over the CRB, from 1000 to 0.1 hPa, can return the net freshwater flux ($E - P$) into the air mass that reached the target basin

(Stohl and James, 2005). In a region, when $(E - P) < 0$, moisture loss prevails in the atmospheric column (i.e. precipitation exceeds evaporation), and the contrary is true (i.e. moisture is retained in the column) when $(E - P) > 0$. In this study, we focused on the computation of $(E - P) < 0$, assumed to represent the contribution to P from each source. This method has been successfully applied in several studies worldwide, especially for humid tropical regions, including the Amazonia (Drumond et al., 2014; Sorí et al., 2018), the Indian subcontinent (Ordoñez et al., 2012), the Sahel (Nieto et al., 2006), and the CRB (Sorí et al., 2017).

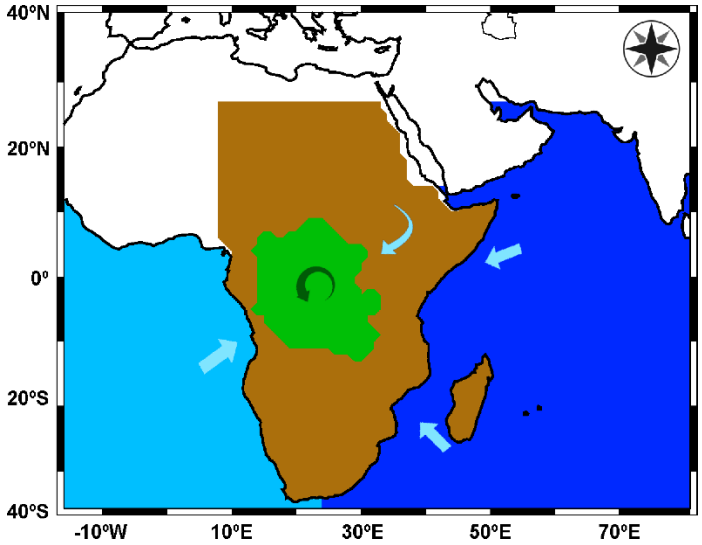

Figure 2. Geographical location of the CRB (green) and regions selected as potential sources of moisture to the CRB: The Atlantic Ocean (light blue), the Indian Ocean (blue), part of the African continent (brown), and the CRB (green). Arrows indicate the paths of predominant moisture fluxes entering the CRB.

Dyer et al. (2017) used a modified version of the National Center for Atmospheric Research Community Earth System Model to track moisture for user-defined regions. Their results showed that the CRB receives moisture mainly from the IO up to 120°E, the CRB itself, the African landmass surrounding the CRB, and the eastern equatorial AO. Similar results were found by Sorí et al. (2017), who utilised a Lagrangian approach. However, Sorí et al. (2017) found that from the Indian Ocean, two main moisture source regions were constrained; the Arabian Sea and the area surrounding Madagascar up to 80°E. In accordance with these findings, West Africa was not considered to be a moisture source for the CRB in this study. Central Africa is an important source of moisture for rainfall in the Sahel and West Africa (van der Ent et al., 2010). Based on these arguments, we established the boundaries of the sources considered in this study (Figure 2).

2.3 Statistical analyses

SPI and SPEI values can be affected by the autocorrelation of the input variables and the effects of moving sums and averages (Páscoa et al., 2017). To avoid this effect in determining drought trends, a modified Mann–Kendall test (Hamed and Rao, 1998) was used. To perform the trend analyses for the rest of the series, the standard Mann–Kendall test (Mann, 1945; Kendall, 1975; Hipel and McLeod, 1994) was utilised.

The modified and standard Mann–Kendall tests are nonparametric in which the null hypothesis, H_0, is that the data come from a population with independent realisations and identical distributions. The alternative hypothesis, H_a, is that the data are monotonic. To complement this analysis, Sen's Slope (Sen, 1968) was also applied. Using a simple linear regression, the coefficient of determination (R^2) was calculated, which shows the proportion of the variance in the dependent variable (severity of drought episodes) that was predictable with respect to the independent variable (contributions from the AO, IO, AF, and CRB). A Student's *t*-test with an α-level of 95% was used to validate the statistical significance of the regression coefficient.

2.4 Data

To calculate the SPI, monthly gridded *P* from the Climate Hazards Center InfraRed Precipitation with Station data (CHIRPS) v2.0 (Funk et al., 2015), available for the period between 1981 and 2018, was used. This dataset combines 0.05°-resolution satellite imagery with in situ station data to create gridded rainfall time series for trend analysis and drought monitoring. To obtain the SPEI, the CHIRPS *P* and PET gridded values from TerraClimate datasets (Abatzoglou et al., 2018) were utilised. We decided to use *PET* instead of the Actual Evapotranspiration (Eta) since, under drought conditions, plants can avoid water loss by closing their stomata, thereby reducing the Eta. Consequently, Eta is not a good indicator of drought stress. TerraClimate is a global database with a high spatial resolution (1/24°, ~4 km) that is obtained using climate-aided interpolation of the Climatic Research Unit (CRU) Ts4.0 data (Harris et al., 2020). Results of Dyer et al. (2017) showed that the seasonal cycle of *P* over the CRB in the CRU TSv.3.21 datasets (Harris et al., 2014) for the period 1980–2000 perfectly match that revealed by the Global Precipitation Climatology Center (GPCP) (Schneider et al., 2015) and the Global Precipitation Climatology Project (GPCP) (Adler et al., 2003) datasets. Nevertheless, CRU Ts4.0 is a datasets derived by the interpolation of monthly climate anomalies from networks of weather station observations, and uses climatological values for grids where long-term observation stations do not exist. It occurs in regions like CEA (5°S–5°N, 12.5–30°E; Washington et al., 2013), wherein the number of rain gauges drastically decreased after 1980, perhaps resulting in the representation of incorrect climate signals in the CRB and other areas. To resolve this problem, TerraClimate also utilises datasets from the Japanese 55-year Reanalysis datasets (JRA-55) (Kobayashi et al., 2015; Harada et al., 2016).

The FLEXPART global outputs utilised here were calculated at the Environmental Physics Laboratory at the University of Vigo, Spain. To run this model, it was necessary to employ global three- and two-dimensional datasets, including the surface pressure, 10-m horizontal wind components, total cloud cover, 2-m temperature and dew point temperature, large-scale and convective precipitation, sensible heat flux, and east/west and north/south surface stresses available at 6-h intervals at 1° horizontal resolutions over 61 vertical levels from 0.1–1000 hPa from ERA-Interim reanalysis datasets (Dee et al., 2011); the topography was also considered.

3. Results and discussion

3.1 Temporal evolution of dry and wet conditions

Figure 3 shows the dry and wet conditions for the period between 1981 and 2018, according to the categories listed in Table 1 at different scales of the SPI and SPEI (from 1–24 temporal scales). Visual

analysis of this figure reveals that the most frequent and intense drought conditions, according to all SPI and SPEI temporal scales, affected the CRB from 1983–1984, 1992–1994, 2004–2005, 2009–2012, and after 2015. There are some differences between the magnitudes of the SPI and SPEI values for some drought periods, such as the end of 1993 and 1994, and after 2015. As expected, these differences occur due to the influence of the PET. Previous studies have also revealed that compared to the period from 1951–1980, meteorological droughts from 1981–2016 were more severe for both SPEI-12 and SPI-12 (i.e. the SPEI and SPI at 12-month timescales) in the CRB (Spinioni et al., 2019). Figure 3 highlights the strong dry conditions in 2015 and 2016, particularly shown by the SPEI (Figure 3b), which indicate the role of PET on modulating drought severity in the CRB. Intense drought conditions associated with the 2015–2016 El Niño event affected the forests, resident livelihoods, and economic growth of the Congo, as well as most of central and southern Africa (Baudoin et al., 2017; Wigneron et al., 2020). A trend analysis of the SPI and SPEI series at scales of 1, 3, 6, 12, 18, and 24 months throughout the study period revealed a similar tendency toward drier conditions, all of which were statistically significant except for the SPI-1 (Table 2). This uninterrupted trend toward drier conditions has been reported many times in the literature.

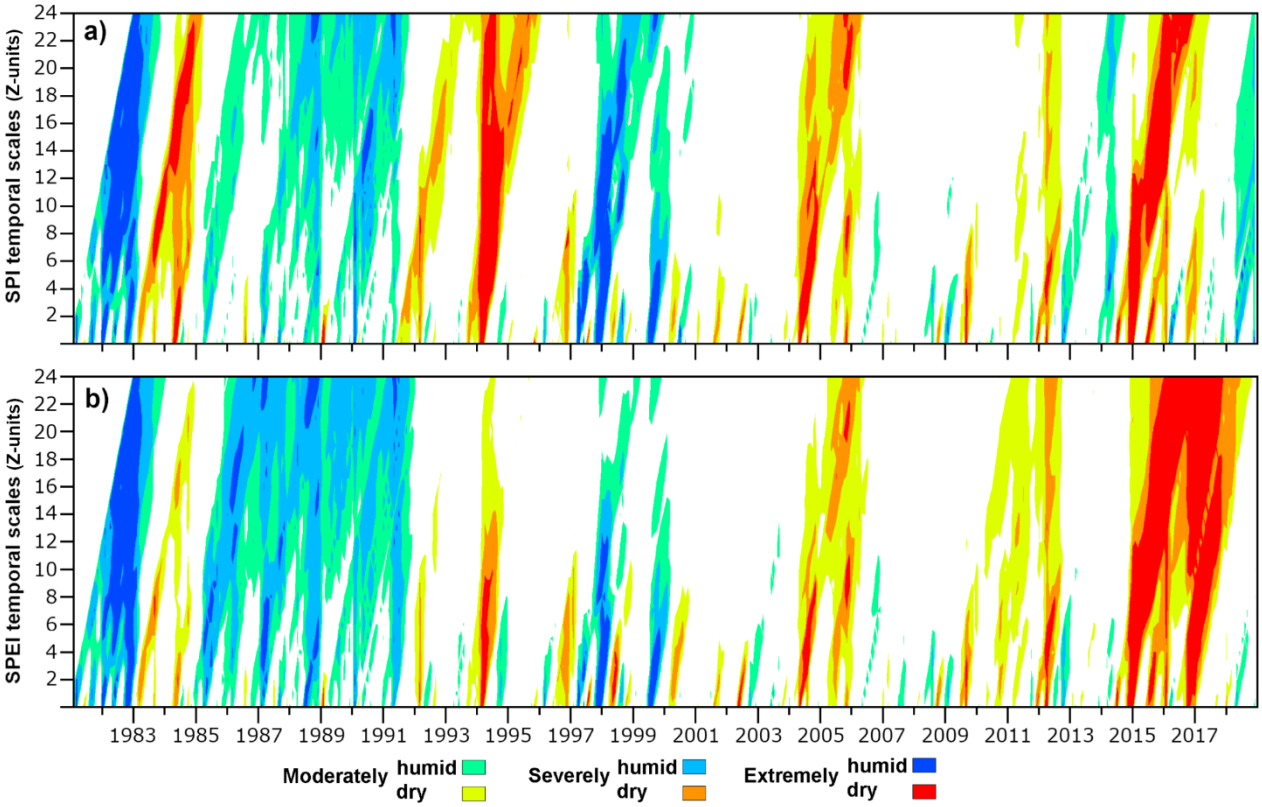

Figure 3. Temporal evolution of the SPI (a) and SPEI (b) at timescales of 1–24 months for 1981–2018 in the CRB. Yellow, orange, and dark red colours represent moderate, severe, and extreme drought conditions, respectively.

Table 2. Statistical indicators of the Mann–Kendall and Sen's Slope test for the trend assessment of SPEI-1, -3, -6, -12, -18, and -24-month time series from 1981–2018.

	SPI			SPEI		
Timescale (months)	***Z***	**Slope**	***p*-value**	***Z***	**Slope**	***p*-value**
1	-1.2731	-0.00046	0.2030	-4.3108	-0.00162	1.6e-05
3	-2.8732	-0.00106	0.4e-03	-7.2673	-0.00271	3.6e-13
6	-4.0933	-0.00159	4.2e-05	-9.8371	-0.00370	2.2e-16
12	-5.9448	-0.00236	2.7e-09	-13.347	-0.00500	2.2e-16
18	-6.5329	-0.00270	6.4e-11	-15.094	-0.00555	2.2e-16
24	-7.2855	-0.00310	3.2e-13	-16.212	-0.00611	2.2e-16

In terms of the spatial trends, previous studies have also shown that most of the patterns of rainfall over CEA from April–June exhibit linear trends (mm d^{-1} $decade^{-1}$) for the period between 1950 and 2014 from the GPCC data, and between 1979 and 2014 from the GPCP data, they exhibit decreasing trends (Hua et al., 2016). Only precipitation values are necessary to calculate the SPI; an increase or decrease in precipitation relative to the historical average is reflected as an increase in wet or dry conditions, respectively. However, as discussed in section 1, the CRB is home to the second largest tropical forest on Earth, which serves as an enormous energy converter, induced by the absorption of solar energy and evaporation processes (Mahé et al., 2005). Forests convert water into water vapour and provide shade more than any other vegetation cover, which can reduce the direct downward shortwave radiation that reaches the surface, leading to cooler surface temperatures (de Wasseige et al., 2015); at the same time, absorption of solar energy limits heating and vaporises water that root systems can extract from the soil (Monteny, 1987). According to Zhou et al. (2014) and Ugbaje and Bishop (2020), the SPEI is an indicator of variations in soil moisture, which is directly related to crop production and rainforest greenness in the CRB. Therefore, we focused on the SPEI rather than the SPI to further investigate drought phenomena in the CRB.

A spatial trend analysis was conducted for the SPEI-1 and SPEI-12 at each grid point within the CRB for the period from 1981–2018 (Figure 4). At these time scales, the negative values of the SPEI were associated with meteorological and long-term drought. The results also revealed that negative trends prevailed across the basin. The critical areas for SPEI-1 were the northern area and parts of the central and southern basin (Figure 4a); meanwhile, significant negative trends in SPEI-12 were observed across almost all of the CRB, with the exception of the western central zone around the mouth of the Congo River, a small area in the north of the basin, and in the southeast (Figure 4b). Our findings are in accordance with those of Spinoni et al. (2019), who revealed the key role of temperature on drought trends over most of Africa. The results also showed that the worst combination of dynamics (i.e. precipitation decrease and PET increase) occurred for drying from 1981–2016, over most of CEA and the entire CRB. Moreover, similar to Spinoni et al. (2019), we found that prevailed a negative trend for the P and a positive trend for PET from 1981–2018 (Figure S1) for the CRB. Most of the negative trends in the SPEI-1 and SPEI-12 in the northern half of the CRB coincide with the dense, humid Congo Rainforest.

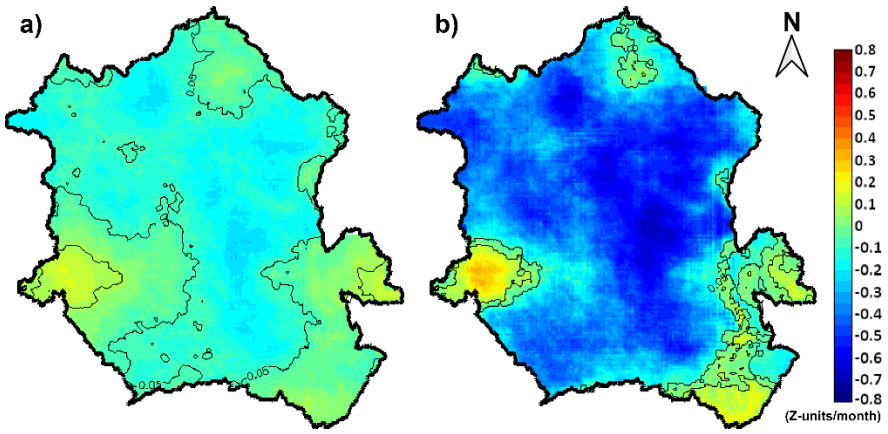

Figure 4. Trends of (a) SPEI-1 and (b) SPEI-12 from 1981–2018. Significant values ($p < 0.05$) are enclosed by continuous lines.

3.2 Moisture contributions to precipitation over the CRB

The contribution of climatological moisture to precipitation over the CRB from each of the source regions shown in Figure 2 are shown as percentages in Figure 5. As can be seen, > 60% of the total moisture was lost in air masses as they were modelled forward in time from the same basin — in agreement with the results of Sorí et al. (2017). The rest of the contribution, from greatest to least, occurred from the rest of the African continent (AF), followed by the IO and AO. These results confirm the importance of continental sources and local recycling. According to van der Ent et al. (2010, 2011), in CEA, the evaporation recycling ratio (i.e. the amount of evaporated water that falls on land versus over the oceans) is one of the highest worldwide. Furthermore, the IO is more important in terms of the total moisture contribution than the AO, in accordance with the results of Dyer et al. (2017), who proposed that much of the moisture transported from the Atlantic into the CRB is recirculated back over the Atlantic in the lower troposphere. For convenience, we used the modulus of the values of $(E - P) < 0$ to calculate the correlations with P series over the basin. The results showed that the best correlations between monthly $\left|(E - P) < 0\right|$ series were obtained in air masses from the CRB, IO, and AF.

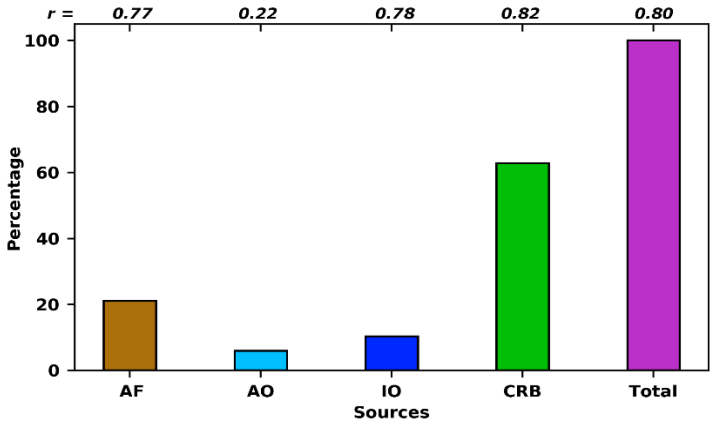

Figure 5. Contribution (%) of climatological moisture to precipitation over the CRB supplied by the AF, AO, IO, and the CRB itself from 1981–2018. Here, *r*-values indicate the correlations between each series

of $|(E-P)<0|$ and P series from CHIRPS.

The monthly correlations between the series of $|(E-P)<0|$ computed from each source with the 1- to 24-month SPEI timescales are shown in Figure 6. Values greater than those represented by the stippled lines within each graph are statistically significant at $p < 0.05$. The correlations between the contributions of moisture from the AO and the IO with the SPEI-1 to SPEI-24 in the CRB were mostly positive for all temporal scales (Figure 6a, 6b). However, significant values appeared at 1–3-month timescales of the SPEI, and at longer timescales from April–September for the AO and from April–July for the IO. These months were characterised by the lowest rainfall in the year; thus, high correlations over longer SPEI timescales (from 6 to 24 months) indicate that total moisture loss over the basin can modulate the accumulated dry/wet conditions from several months before, even at a time scale of 2 years. At these time scales, the SPEI is usually associated with hydrological droughts. Vicente-Serrano et al. (2012) also found that hydrological droughts in the CRB, according to the Standardised Streamflow Index, are closely related to climatic droughts computed at timescales between 3 and 10 months by the SPEI. The correlation between terrestrial moisture supplies from the AF and CRB and SPEI are better than those of oceanic moisture and the SPEI at all timescales throughout the year, which is contrary to that observed for the AO and IO, during the rainiest months (October to March) (Figure 6c, 6d). The findings of Tomas-Burguera et al. (2020) revealed that high precipitation in humid regions like the CRB can modulate the impacts of the interannual variability of *PET* on drought severity, although some influence can also be found in dry years.

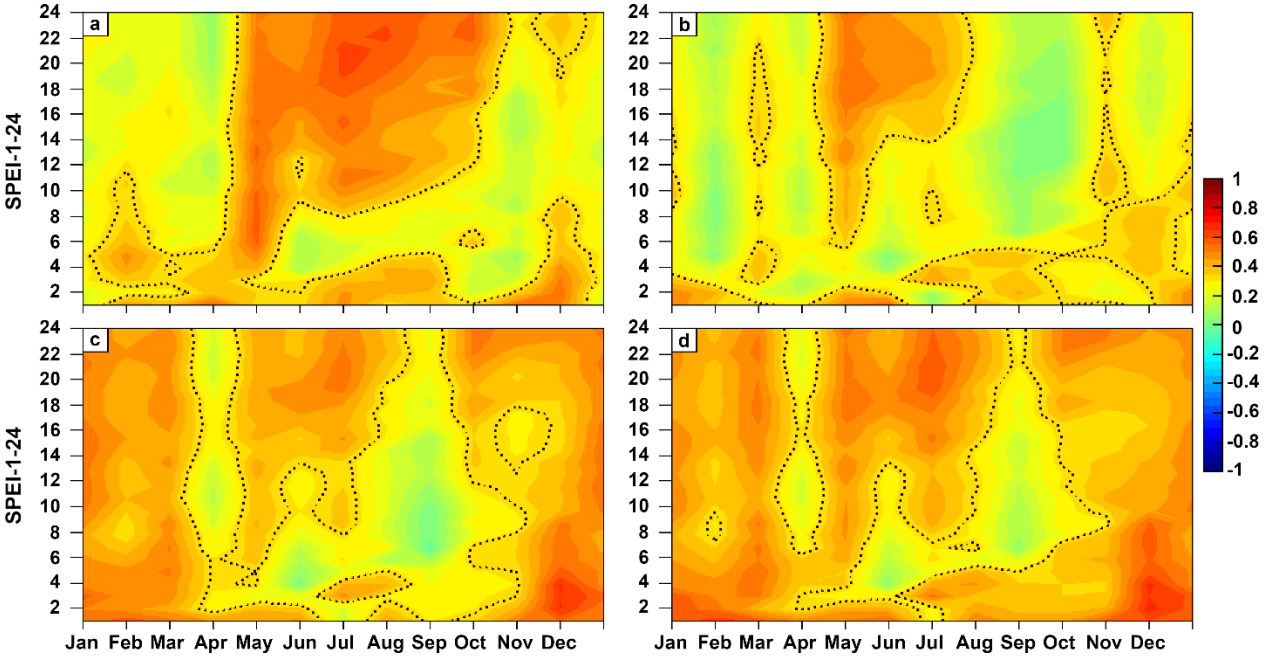

Figure 6. Temporal correlations between monthly anomalies of $|(E-P)<0|$ computed over the CRB from the (a) AO, (b) IO, (c) AF, and (d) CRB with monthly SPEI values at 1–24-month timescales from 1981–2018. Statistically significant values ($p < 0.05$) are greater than those represented by a dashed line.

Figure 7 shows the accumulated anomalies of $|(E-P)<0|$ computed over the CRB in the forward

analysis from each source and for each of the meteorological drought episodes identified in the study period (N = 53). A visual analysis reveals that in most of the episodes, there was a decrease in the moisture contributed from the source regions, except in nine episodes for the AO, 13 for AF and the CRB, and 17 for the IO. The greatest anomalies in all of the episodes occurred in the moisture contributed from the CRB, followed by the rest of the AF. Figure 7 highlights the 48th and 51st episodes because they represent the greatest total anomalies. These episodes of drought affected the CRB from September 2014 to January 2015 (five months; episode 48) and from May 2016 to January 2017 (nine months; episode 51), which is in accordance with prevailing drought conditions observed after 2015 (Figure 3b).

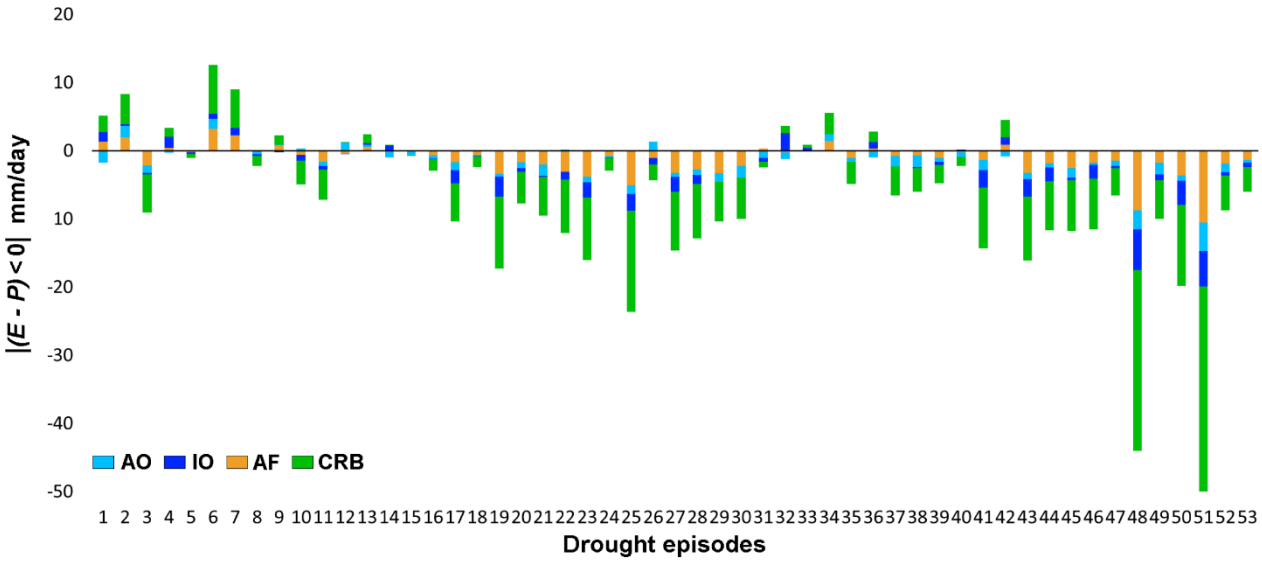

Figure 7. Monthly anomalies of the contributions of moisture from the AO (light blue), IO (dark blue), AF (orange), and CRB (green) accumulated during each drought episode identified over the CRB from 1981–2018.

Supplementary Table 1 shows the dates of every meteorological drought episode, as well as their duration and severity. It was observed that in some episodes, the anomalies were positive from some sources and negative from others, which means that the contribution of moisture from some sources may have a more dominant role than others. This phenomenon was explained by Sorí et al. (2017), who found that the spatial variability in the $\left|(E-P)<0\right|$ patterns over the CRB was influenced by synoptic and dynamic conditions and the geographical locations of the sources.

It is important to know the role of the sources before the onset of drought episodes. Table 3 shows the percentage of months with negative anomalies in the contribution of moisture at the beginning of each drought episode, as well as for the preceding one and two months. Here, we considered the 53 meteorological drought episodes identified with the SPEI-1. As can be seen, > 80% of the months in which the episodes began coincided with negative anomalies in the moisture contributed from the AF and the CRB, followed by 78.8% of the months for contributions from the IO, and 65.4% from the AO. This changed for a month before, when 55.8% and 51.9% of months with negative anomalies in their values of $\left|(E-P)<0\right|$ computed over the CRB were from the IO and AO, respectively — greater percentages than from the terrestrial sources, the AF (50%) and the CRB (44.2%). Two months before the onset of droughts, the percentage was also > 50%, with the minimum shown for the CRB (51.9%). Until now, the results

showed the importance of terrestrial sources; however, the fact that in a greater number of months, a decrease occurred in the contribution of moisture from oceanic sources than from terrestrial sources indicates that both the IO and AO can play a deterministic role in the onset of meteorological drought episodes, though this should be investigated further.

Table 3. Percentage of months with negative anomalies in the moisture contributed from each source at the onset of each drought episode and during the previous 1 and 2 months.

Negative anomalies (%)				
	CRB	**AF**	**AO**	**IO**
Onset	82.7	80.8	78.8	65.4
Onset – 1 month	44.2	50.0	51.9	55.8
Onset – 2 months	51.9	57.7	55.8	57.7

The values of the total $\left|(E - P) < 0\right|$ anomalies during drought episodes presented in Figure 7 may be related to the severity of the episode. Thus, possible relationships between the severity of meteorological drought episodes and variations in moisture supplied from the AO, IO, AF, and CRB were investigated through a simple linear regression (Figure 8). The highest R^2 (= 0.42) was found between severity and $(E - P) < 0$ series of anomalies computed in the model from the CRB (Figure 8d). This relationship was statistically significant at $p < 0.05$ and indicates that 42% of the variability in the severity of drought episodes could be explained by variations in the moisture supplied from the CRB itself. The rest of the regressions in Figure 8 exhibit lower explained variances, although these values are also statistically significant. The R^2 values decreased similarly to the percentages of the total contributions shown in Figure 5 (i.e. CRB > AF > IO > AO), which suggests that the severity of the episodes is related to the magnitude of moisture contributed from each of the source regions.

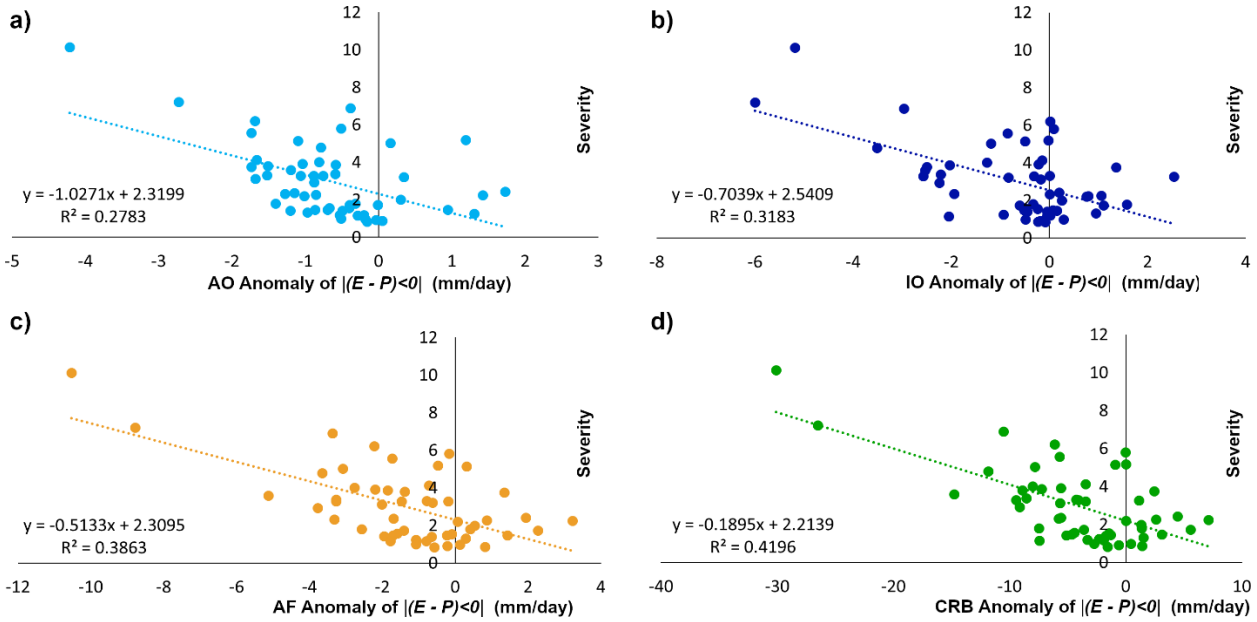

Figure 8. Scatterplot: anomalies in moisture contributed from the (a) AO, (b) IO, (c) AF, and (d) CRB (x-axis, mm/day) and the severity of drought episodes. Discontinued lines are the corresponding regression lines. Period 1981 – 2018.

A trend analysis for the $|(E - P) < 0|$ series revealed that all contribution sources experienced a statistically significant decrease from 1981–2018 (Table 4). Consequently, the slope in the total moisture contribution experienced a decrease of 0.0162 mm d^{-1} $month^{-1}$. In this analysis, the major slope represents the moisture contribution from the AF (-0.0032 mm d^{-1} $month^{-1}$). Nevertheless, considering the important role of the CRB in its own hydroclimate, we plotted the temporal evolution of monthly $|(E - P) < 0|$ anomalies and the moisture contribution from the CRB itself (Figure 9). From 1995–2004 and from 2012–2016, it was observed that negative anomalies prevailed in this series. Compared with Figure 3b, the first of these periods coincided with intermittent drought conditions at short and moderate SPEI timescales, and the second period was in agreement with the most intense drought that affected the CRB in the study period.

Table 4. Trends of $|(E - P) < 0|$ series over the CRB from each source between 1980 and 2018. Statistically significant ($p < 0.05$) trends are denoted by an asterisk (*).

Source	***Z***	**Slope** (mm/day)	***p*-value**
AF	-5.91	-0.0032	3.384e-09*
AO	-6.42	-0.0015	1.326e-10*
IO	-3.25	-0.0010	0.001145*
CRB	-6.07	-0.0100	1.271e-09*
Total	-6.07	-0.0162	1.212e-09*

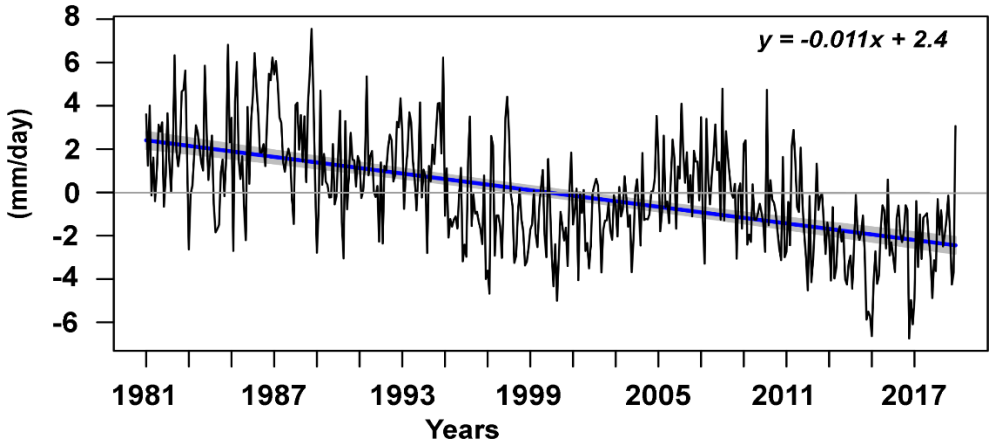

Figure 9. Temporal evolution of the $|(E - P) < 0|$ anomalies computed over the CRB in a forward experiment for the moisture provision from the CRB itself (1981–2018). The blue line shows the linear trend of the series and the shaded area shows the 95% confidence interval.

A spatial trend analysis was performed for the moisture contributed from each source (Figure 10). From the AO (Figure 10a), a small region with significant positive trends matches the region of the mouth of the Congo River, while negative trends prevail over the rest of the basin, particularly over the northwest. The trend of $\left|(E - P) < 0\right|$ calculated from the IO is also primarily negative, with significant trends in the northern half of the CRB, which were more intense in the central and eastern parts (Figure 10b). An increase in the moisture contributed from the IO was also observed in the west-central part of the CRB, and over the southeast. For the AF and the CRB itself (Figure 10c, d), it was also observed that negative trends prevailed in the northern half of the CRB, where several subbasins, such as the Middle Congo, Oubangui, Ruki, and Sangha, and the northern Upper Congo River, are located; these tributaries are very important for the Congo River (Becker et al., 2014). The greatest and most significant negative anomalies in moisture contributions from the CRB itself were observed in the regions occupied by humid rainforests. In contrast, intense and significant positive trends in the moisture contributions were observed from the CRB in the west-central CRB over the mouth of the Congo River. The spatial configuration of the trends is similar to the patterns of the SPEI-1 and SPEI-12 (Figure 5a, b). Greater negative trends in moisture loss over the northern Congo Rainforest also coincided with observational evidence of a widespread decline in forest greenness over the last decade in the CRB (Zhou et al., 2014). In this study, the air masses residing over the entire CRB were modelled forward in time and the net freshwater was computed along the trajectories. A more detailed study that only considers the Congo Rainforest should be conducted to clarify the contribution of this region on the variability in local and remote rainfall and the occurrence of dry/wet conditions.

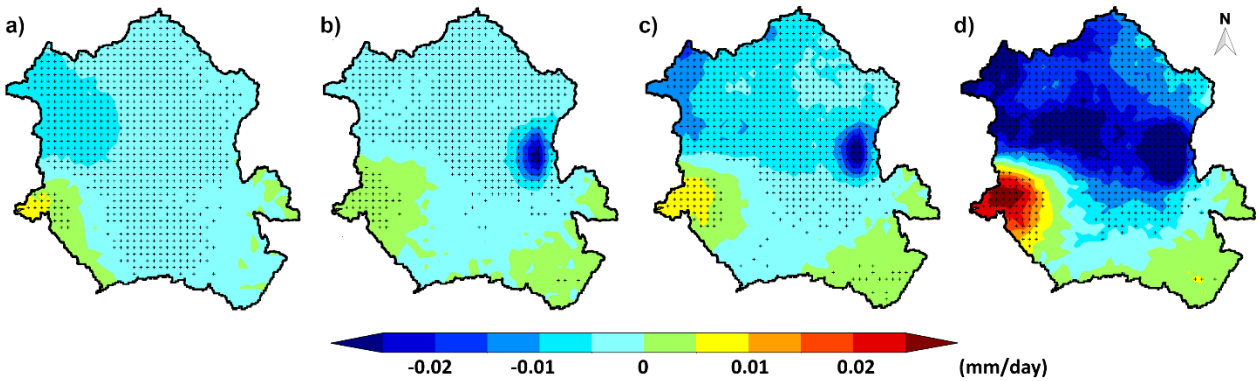

Figure 10. Trends of $\left|(E - P) < 0\right|$ calculated over the CRB for air masses modelled forward in time from the (a) AO, (b) IO, (c) AF, and (d) CRB. Significant values ($p < 0.05$) are denoted by black dots.

4. Conclusions

In this study we found that the CRB experienced a trend toward dryness from 1981–2018, which is in agreement with previous findings for CEA. The SPI and SPEI were utilised to identify and investigate the occurrence of drought conditions in the CRB. The results confirmed the importance of PET in modulating drought conditions, especially for the severe and extreme droughts that affected the CRB from 2015–2017. The spatial trend of the SPEI at short (1 month) and long (12 months) timescales revealed significant decreases in the northern half of the CRB and in parts of the central and southern basin; however, the drying trend according to the SPEI-1 was mainly observed in the northern half of the CRB along the Congo Rainforest.

To investigate the role of moisture transport from the AO, IO, AF, and the CRB itself, we used the Lagrangian model

FLEXPART. The analysis confirmed that the moisture contribution to precipitation from the CRB itself was > 60%. The AF was also an important source of moisture for the CRB. Meanwhile, the moisture contribution to precipitation from the IO was greater than that supplied from the AO. For all sources, we found a decrease in the moisture contributed to the CRB during the study period, especially during meteorological drought episodes. However, positive trends in the moisture contributed from all sources occurred in the west-central part of the basin around the mouth of the Congo River, in accordance with wetting trends.

Our results suggest that decreases in the moisture contributed from the IO and AO, followed by the contributions from the AF and the CRB itself, one month before the onset of drought episodes may be directly correlated. The spatial trends of the $\left|(E-P)<0\right|$ series were very similar to those of the SPEI-1 and SPEI-12, and showed that moisture lost over the CRB in air masses from the AO, IO, AF, and particularly the CRB itself, decreased in the northern half of the basin, over the Congo Rainforest. This suggests that local rainfall generated via recycling decreased, confirming previous findings on the role of decreased precipitation and increased PET in regions of CEA**.** Thus, strong land–plant–atmosphere hydroclimatic feedbacks exist in the CRB and are driven by local and remote conditions. Our future research will explore the spatiotemporal variability in moisture contributions during different seasons and for different subbasins in order to more accurately understand the role of moisture transport from oceanic and terrestrial sources on the occurrence and evolution of dry and wet conditions within the CRB. In the same way, the role of humid forests in contributing to local and remote precipitation will also be investigated.

Acknowledgments

Rogert Sorí acknowledges the postdoctoral grant by the Xunta de Galicia (grant no. ED481B 2019/070). Margarida L. R. Liberato and Milica Stojanovic acknowledge the support received by the project “Weather Extremes in the Euro Atlantic Region: Assessment and Impacts–WEx-Atlantic” (no. PTDC/CTA-MET/29233/2017).

Funding

This work has been financially supported by the Spanish Government within the LAGRIMA project (RTI2018-095772-B-I00). Partial support was also obtained from the Xunta de Galicia under the Project ED431C 2017/64-GRC Programa de Consolidación e Estructuración de Unidades de Investigación Competitivas (Grupos de Referencia Competitiva) and Consellería de Educación e Ordenación Universitaria. All of them cofunding from the ERDF, in the framework of the Operational Program Galicia 2014–2020. Finally, the authors would like to thank two anonymous reviewers for their useful comments and efforts towards improving the manuscript.

References

Abatzoglou, J., Dobrowski, S., Parks, S.A., & Hegewisch, K. C. (2018) TerraClimate, a high-resolution global dataset of monthly climate and climatic water balance from 1958–2015, Sci. Data, 5, 170191. https://doi.org/10.1038/sdata.2017.191.

Adler, R.F. et al. (2003). The Version-2 Global Precipitation Climatology Project (GPCP) Monthly Precipitation Analysis (1979–Present). J. Hydrometeor., 4, 1147–1167, https://doi.org/10.1175/1525-7541(2003)004<1147:TVGPCP>2.0.CO;2.

Alsdorf, D., Beighley, E., Laraque, A., Lee, H., Tshimanga, R., O'Loughlin, F., Mahé, G., et al. (2016). Opportunities for hydrologic research in the Congo Basin, Reviews of Geophysics, 54, 378– 409. https://doi.org/10.1002/2016RG000517

Agnew, C. T. (2000). Using the SPI to identify drought, Drought Netw. News, 2000, 12, 6–12, available at: http://digitalcommons.unl.edu/droughtnetnews/1

Baudoin, M.A., Vogel, C., Nortje, K., & Naik, M. (2017). Living with drought in South Africa: lessons learnt from the recent El Niño drought period. International Journal of Disaster Risk Reduction, 23, 128-137. https://doi.org/10.1016/j.ijdrr.2017.05.005

Becker, M., Da Silva, J.S., Calmant, S., Robinet, V., Linguet, L., & Seyler, F. (2014). Water Level Fluctuations in the Congo Basin Derived from ENVISAT Satellite Altimetry. Remote Sensing, 6(10), 9340-9358. https://doi.org/10.3390/rs6109340

Beguería, S., Vicente-Serrano, S.M., Reig, F., & Latorre, B. (2014). Standardized precipitation evapotranspiration index (SPEI) revisited: Parameter fitting, evapotranspiration models, tools, datasets and drought monitoring. Int. J. Climatol., 34, 3001–3023 https://doi.org/10.1002/joc.3887

Bell, J.P., Tompkins, A.M., Bouka-Biona, C., & Sanda, I.S. (2015). A process-based investigation into the impact of the Congo basin deforestation on surface climate. J. Geophys. Res. Atmos., 120, 5721– 5739. https://doi.org/10.1002/2014JD022586

Chakraborty, S., Jiang, J. H., Su, H., & Fu, R. (2020). Deep convective evolution from shallow clouds over the Amazon and Congo rainforests. J. Geophys. Res. Atmos., 125, e2019JD030962. https://doi.org/10.1029/2019JD030962

Dargie, G.C., Lawson, I.T., Rayden, T.J., Miles, L., Mitchard, E.T.A., Page, S.E., et al. (2019). Congo Basin peatlands: threats and conservation priorities. Mitig Adapt Strateg Glob Change 24, 669–686. https://doi.org/10.1007/s11027-017-9774-8

de Wasseige C., Tadoum M., Eba'a Atyi R. & Doumenge C. (Eds.). (2015). The Forests of the Congo Basin - Forests and climate change. Weyrich. Belgium. 128 p. ISBN: 978-2-87489-355-1. https://agritrop.cirad.fr/578904/1/Forets%20of%20the%20congo%20basin.pdf

Dee, D. P., Uppala, S.M., Simmons, A.J., Berrisford, P., Poli, P., Kobayasji, S., et al. (2011) The ERA-Interim reanalysis: Configuration and performance of the data assimilation system. Q. J. R. Meteorol. Soc., 137, 553–597. https://doi.org/10.1002/qj.828

Drumond, A., Marengo, J., Ambrizzi, T., Nieto, R., Moreira, L., & Gimeno, L. (2014) The role of the Amazon Basin moisture in the atmospheric branch of the hydrological cycle: a Lagrangian analysis, Hydrol. Earth Syst. Sci., 18, 2577–2598. https://doi.org/10.5194/hess-18-2577-2014

Dyer, E.L.E., Jones, D.B.A., Nusbaumer, J., Li, H., Collins, O., Vettoretti, G., & Noone, D. (2017), Congo Basin precipitation: Assessing seasonality, regional interactions, and sources of moisture, J. Geophys. Res. Atmos., 122, 6882–6898, https://doi.org/10.1002/2016JD026240

Edwards, D.C. & McKee, T.B. (1997) Characteristics of 20th century drought in the United States at multiple time scales. Climatology Report 97-2, Department of Atmospheric Science, Colorado State University, Fort Collins, Colorado. https://mountainscholar.org/handle/10217/170176

Eltahir, E.A.B. (1996). Role of vegetation in sustaining large-scale atmospheric circulations in the tropics, J. Geophys. Res., 101(D2), 4255–4268. https://doi.org/10.1029/95JD03632

Funk, C., Peterson, P., Landsfeld, M. et al. (2015). The climate hazards infrared precipitation with stations—a new environmental record for monitoring extremes. Sci Data 2, 150066. https://doi.org/10.1038/sdata.2015.66

Gautier, D., Denis, D. & Locatelli, B. (2016). Impacts of drought and responses of rural populations in West Africa: a systematic review. WIREs Clim Change, 7, 666-681. https://doi.org/10.1002/wcc.411

Gimeno, L., Nieto, R. & Sorí, R. (2020). The growing importance of oceanic moisture sources for continental precipitation. npj Clim Atmos Sci, 3, 27. https://doi.org/10.1038/s41612-020-00133-y

Harada, Y., Kamahori, H., Kobayashi, C., Endo, H, Kobayashi, S., Ota, Y., et al. (2016) The JRA-55 Reanalysis: Representation of atmospheric circulation and climate variability, J. Meteor. Soc. Japan, 94, 269-302, https://doi.org/10.2151/jmsj.2016-015

Harris, I., Jones, P., Osborn, T. & Lister, D. (2014). Updated high-resolution grids of monthly climatic observations – the CRU TS3.10 Dataset. Int. J. Climatol., 34, 623-642. https://doi.org/10.1002/joc.3711

Harris, I., Osborn, T.J., Jones, P. et al. (2020). Version 4 of the CRU TS monthly high-resolution gridded multivariate climate dataset. Sci Data 7, 109. https://doi.org/10.1038/s41597-020-0453-3

Hamed, K.H. & Rao, A.R. (1998) A modified Mann-Kendall trend test for autocorrelated data, Journal of Hydrology, 204, 182–196. https://doi.org/10.1016/S0022-1694(97)00125-X

Hipel, K.W. & McLeod, A.I. (1994). Time Series Modelling of Water Resources and Environmental Systems. Elsevier Science. https://doi.org/10.1002/iroh.19950800107

Hua, W., Zhou, L., Chen, H., Nicholson, S.E., Raghavendra, A., & Jiang, Y. (2016). Possible causes of the Central Equatorial African long-term drought. Environ. Res. Lett., 11, 124002 https://doi.org/10.1088/1748-9326/11/12/124002

Hua, W., Zhou, L., Chen, H., Nicholson, S.E., Jiang, Y., & Raghavendra, A. (2018) Understanding the Central Equatorial African long-term drought using AMIP-type simulations. Climate Dynamics, 50, 1115–1128. https://doi.org/10.1007/s00382-017-3665-2

Jiang, Y., Zhou, L., Tucker, C.J., Raghavendra, A., Hua, W., Liu, Y., & Joiner, J. (2019). Widespread increase of boreal summer dry season length over the Congo rainforest. Nature Climate Change, 9, 617–622. https://doi.org/10.1038/s41558-019-0512-y

Kamali, B., Abbaspour, K.C., Lehmann, A., Wehrli, B., & Yang, H. (2018) Spatial assessment of maize physical drought vulnerability in sub-Saharan Africa: Linking drought exposure with crop failure. Environ. Res. Lett., 13, 074010. https://doi.org/10.1088/1748-9326/aacb37

Kendall, M.G. 1975. Rank Correlation Methods, 4th edition, Charles Griffin, London.

Kobayashi, S., Ota, Y., Harada, Y., Ebita, A., Moriya, M., Onoda, H., et al. (2015). The JRA-55 Reanalysis: General specifications and basic characteristics. J. Meteor. Soc. Japan, 93, 5-48. https://doi.org/10.2151/jmsj.2015-001

Koutrouvelis, I.A., & Canavos, G.C. (1999). Estimation in the Pearson type 3 distribution, Water Resour. Res., 35(9), 2693–2704. https://doi.org/10.1029/1999WR900174

Mahé, G., Servat, E., & Maley, J. (2004). Climatic variability in the Tropics. In: Forest, Forests, Water and People in the Humid Tropics: Past, Present and Future Hydrological Research for Integrated Land and Water Management. M. Bonell, & Bruijnzeel, L.A. (Eds) Cambridge University Press, 267-286.

Mann, H.B. (1945). Non-parametric tests against trend, Econometrica 13:163-171.

Masih, I., Maskey, S., Mussá, F.E.F., & Trambauer, P. (2014). A review of droughts on the African continent: a geospatial and long-term perspective, Hydrol. Earth Syst. Sci., 18, 3635–3649. https://doi.org/10.5194/hess-18-3635-2014

McKee, T., Doesken, N., & Kleist, J. (1993) The relationship of drought frequency and duration to time scales, Eighth Conference on Applied Climatology, 17–22 January, Anaheim, California. https://www.droughtmanagement.info/literature/AMS_Relationship_Drought_Frequency_Duration_Time_Scales_1993.pdf

Megevand, C., Mosnier, A., Hourticq, J., Sanders, K., Doetinchem, N., Streck, C. (Eds.) (2013). Deforestation Trends in the Congo Basin: Reconciling Economic Growth and Forest Protection. Washington, DC: World Bank. 2013. https://doi.org/10.1596/978-0-8213-9742-8

Monteny, B.A. (1987). "Contribution á létude des interactions vegeation-atmosphere en milieu tropica, humide "- Importance du rôle du Systeme forestier dans le recyclage des eaux de pluie. 17Op. These de Doctorat d'Etat, Universite de Paris XI, Orsay

Niang, I., O.C. Ruppel, M.A. Abdrabo, A. Essel, C. Lennard, J. Padgham, and P. Urquhart, 2014: Africa. In: Climate Change 2014: Impacts, Adaptation, and Vulnerability. Part B: Regional Aspects. Contribution of Working Group II to the Fifth Assessment Report of the Intergovernmental Panel on Climate Change [Barros, V.R., C.B. Field, D.J. Dokken, M.D. Mastrandrea, K.J. Mach, T.E. Bilir, M. Chatterjee, K.L. Ebi, Y.O. Estrada, R.C. Genova, B. Girma, E.S. Kissel, A.N. Levy, S. MacCracken, P.R. Mastrandrea, and

L.L.White (eds.)]. Cambridge University Press, Cambridge, United Kingdom and New York, NY, USA, pp. 1199-1265. https://www.ipcc.ch/site/assets/uploads/2018/02/WGIIAR5-Chap22_FINAL.pdf

Nicholson, S. E., Funk C., & Fink, A.H. (2018) Rainfall over the African continent from the 19th through the 21st century. Global and Planetary Change., 165, 114-127. https://doi.org/10.1016/j.gloplacha.2017.12.014

Nicholson, S.E. (2018). The ITCZ and the Seasonal Cycle over Equatorial Africa. Bull. Amer. Meteor. Soc., 99, 337–348. https://doi.org/10.1175/BAMS-D-16-0287.1

Nieto, R., Gimeno, L., & Trigo, R. M. (2006). A Lagrangian identification of major sources of Sahel moisture, Geophys. Res. Lett., 33, L18707. https://doi.org/10.1029/2006GL027232

Nogherotto, R., Coppola, E., Giorgi, F. & Mariotti, L. (2013). Impact of Congo Basin deforestation on the African monsoon. Atmos. Sci. Lett, 14, 45-51. https://doi.org/10.1002/asl2.416

Numaguti, A. (1999). Origin and recycling processes of precipitating water over the Eurasian continent: Experiments using an atmospheric general circulation model, J. Geophys. Res., 104(D2), 1957– 1972, doi:10.1029/1998JD200026.

Ordoñez, P., Ribera, P., Gallego, D., & Peña-Ortiz, C. (2012). Major moisture sources for Western and Southern India and their role on synoptic-scale rainfall events, Hydrological Processes, 26, 3886-3895. https://doi.org/10.1002/hyp.8455

Palmer, W.C. Meteorological Drought. 1965. Available online: https://www.ncdc.noaa.gov/temp-and-precip/drought/docs/palmer.pdf

Páscoa, P., Gouveia, C.M., Russo, A., & Trigo, R.M. (2017) Drought Trends in the Iberian Peninsula over the Last 112 Years, Adv. Meteorol., 1-13. https://doi.org/10.1155/2017/4653126

Pokam, W.M., Djiotang, L.A.T., & Mkankam, F.K. (2012). Atmospheric water vapor transport and recycling in Equatorial Central Africa through NCEP/NCAR reanalysis data. Climate Dynamics, 38, 1715-1729. https://doi.org/10.1007/s00382-011-1242-7

Raghavendra, A., Zhou, L., Roundy, P.E., Jiang, Y., Milard, S.M., Hua, W., & Xia, G. (2020). The MJO's impact on rainfall trends over the Congo rainforest. Climate Dynamics, 54, 2683–2695. https://doi.org/10.1007/s00382-020-05133-5

Sen, P.K. (1968). Estimates of the Regression Coefficient Based on Kendall's Tau. Journal of the American Statistical Association, 63, 1379–1389. https://www.tandfonline.com/doi/pdf/10.1080/01621459.1968.10480934?needAccess=true

Singh V.P. (1998) Three-Parameter Log-Logistic Distribution. Entropy-Based Parameter Estimation in Hydrology, 30, 297-311. https://doi.org/10.1007/978-94-017-1431-0_18

Sonwa, D.J., Oumarou Farikou, M., Martial, G., & Félix, F.L. (2020) Living under a Fluctuating Climate and a Drying Congo Basin. Sustainability, 12, 2936. https://doi.org/10.3390/su12072936

Sorí, R., Nieto, R., Vicente-Serrano, S.M., Drumond, A. & Gimeno, L. (2017) A Lagrangian perspective of the hydrological cycle in the Congo River basin. Earth Syst. Dyn., 8, 653–675. https://doi.org/10.5194/esd-8-653-2017

Sorí, R., Marengo, J., Nieto, R., Drumond, A., & Gimeno L. (2018). The Atmospheric Branch of the Hydrological Cycle over the Negro and Madeira River Basins in the Amazon Region, Water, 2018, 10(6), 738. https://doi.org/10.3390/w10060738

Spinoni, J., Barbosa, P., De Jager, A., McCormick, N., Naumann, G., Vogt, J.V., et al. (2019). A new global database of meteorological drought events from 1951 to 2016. Journal of Hydrology: Regional Studies, 22, 100593. https://doi.org/10.1016/j.ejrh.2019.100593

Stohl, A., & James, P. (2004). A Lagrangian analysis of the atmospheric branch of the global water cycle. Part I: Method description, validation, and demonstration for the August 2002 flooding in central Europe. J. Hydrometeor., 5, 656–678. https://doi.org/10.1175/1525-7541(2004)005<0656:ALAOTA>2.0.CO;2

Stohl, A., & James, P. (2005). A Lagrangian analysis of the atmospheric branch of the global water cycle. Part II: Moisture transports between Earth's ocean basins and river catchments. J. Hydrometeor., 6, 961–984. https://doi.org/10.1175/JHM470.1

Tomas-Burguera, M., Vicente-Serrano, S.M., Peña-Angulo, D., Domínguez-Castro, F., Noguera, I., El Kenawy, A. (2020). Global Characterization of the Varying Responses of the Standardized Precipitation Evapotranspiration Index to Atmospheric Evaporative Demand. J. Geophys. Res. Atmos.,125(17), e2020JD033017. https://doi.org/10.1029/2020JD033017

Tyukavina, A., Hansen, M.C., Potapov, P., Parker, D., Okpa, C., Stehman, S.V., et al. (2018). Congo Basin forest loss dominated by increasing smallholder clearing. Science Advance, 4(11), eaat2993. https://doi.org/10.1126/sciadv.aat2993

Ugbaje, S.U., & Bishop, T.F. (2020). Hydrological Control of Vegetation Greenness Dynamics in Africa: A Multivariate Analysis Using Satellite Observed Soil Moisture, Terrestrial Water Storage and Precipitation, 9(1), 15. https://doi.org/10.3390/land9010015

van der Ent, R.J., Savenije, H.H.G., Schaefli, B., & Steele-Dunne, S. C. (2010). Origin and fate of atmospheric moisture over continents, Water Resour. Res., 46, 1–12. https://doi.org/10.1029/2010WR009127

van der Ent, R. J. & Savenije, H.H.G. (2011). Length and time scales of atmospheric moisture recycling, Atmos. Chem. Phys., 11, 1853–1863. https://doi.org/10.5194/acp-11-1853-2011

Vicente-Serrano, S. M. (2006). Differences in Spatial Patterns of Drought on Different Time Scales: An Analysis of the Iberian Peninsula. Water Resources Management, 20,37-60.

https://doi.org/10.1007/s11269-006-2974-8

Vicente-Serrano, S. M., Beguería, S. & López-Moreno, J. I. (2010). A multiscalar drought index sensitive to global warming: The standardized precipitation evapotranspiration index. J. Climate, 23, 1696–1718. https://doi.org/10.1175/2009JCLI2909.1

Vicente-Serrano, S.M., Beguería, S., Gimeno, L., Eklundh, L.,Giuliani, G., Weston, D., et al. (2012). Challenges for drought mitigation in Africa: The potential use of geospatial data and drought information systems, Applied Geography, 34, 471-486. https://doi.org/10.1016/j.apgeog.2012.02.001

Washington R, James R, Pearce H, Pokam WM, & Moufouma-Okia W. (2013). Congo Basin rainfall climatology: can we believe the climate models?. Philos Trans R Soc Lond B Biol Sci., 368(1625), 20120296. https://doi.org/10.1098/rstb.2012.0296

Wigneron, J.P., Fan, L., Ciais, P., Bastos, A., Brandt, M., Chave, J., et al. (2020). Tropical forests did not recover from the strong 2015–2016 El Niño event. Science Advances, 6, eaay4603. https://doi.org/10.1126/sciadv.aay4603

Wilhite, D.A. (1992). "Drought". Drought Mitigation Center Faculty Publications. 64. http://digitalcommons.unl.edu/droughtfacpub/64

Wilhite, D. A., & Glantz, M. H. (1985). Understanding the drought phenomenon: The role of definitions. Water Int., 10, 111–120. https://doi.org/10.1080/02508068508686328

WMO (World Meteorological Organization), 2012: Standardized Precipitation Index User Guide (M. Svoboda, M. Hayes and D. Wood). (WMO-No. 1090), Geneva. Available online: http://www.wamis.org/agm/pubs/SPI/WMO_1090_EN.pdf

WMO and GWP – World Meteorological Organization and Global Water Partnership: Handbook of Drought Indicators and Indices, in: Integrated Drought Management Programme (IDMP), Integrated Drought Management Tools and Guidelines Series 2, edited by: Svoboda, M. and Fuchs, B. A., Geneva, 2016 Available online: https://www.droughtmanagement.info/literature/GWP_Handbook_of_Drought_Indicators_and_Indices_2016.pdf

WWF (World Wide Fund For Nature). Rivers of the Green Heart of Africa. Available at: https://www.wwf-congobasin.org/congo_basin_at_a_glance/area/ecosystems/rivers/. Last access October 13, 2020.

Zhou, L., Tian, Y., Myneni, R.B., Ciais, P., Saatchi, S., Liu, Y.Y., et al. (2014). Widespread decline of Congo rainforest greenness in the past decade. Nature, 509, 86–90. https://doi.org/10.1038/nature13265